Quasi-one-dimensional polaronic states due to the preferential reduction in the $Li_{1+x}V_3O_8$ insertion electrode

Quasi-one-dimensional polaronic states due to the preferential reduction in the $Li_{1+x}V_3O_8$ insertion electrode

Masashige Onoda and Isao Amemiya

Institute of Physics, University of Tsukuba, Tennodai, Tsukuba 305-8571, Japan

Abstract
The structural and electronic properties of the $Li_{1+x}V_3O_8$ insertion electrode, where $0 \leqslant x < 0.4$, have been explored by means of x-ray four-circle diffraction and through measurements of electrical resistivity, thermoelectric power, magnetization and electron paramagnetic resonance. Detailed structure refinements for $x = 0.06$ and 0.29 reveal the preferential and partial reduction of V ions which may give rise to low-dimensional electronic properties. The composition with $x = 0$ exhibits a quasi-one-dimensional polaronic transport in the localized states of band tails due to the slight deficiency of oxygen atoms. For $x > 0.1$ with nearly stoichiometric oxygen atoms, small polarons exist without carrier-creation energy at high temperatures, while at low temperatures the conduction may be of variable-range hopping (VRH) type. For $x > 0.2$, one-dimensional magnetic properties appear due to sizable exchange couplings and order–disorder effects of additional Li ions may lead to significant change of transport properties. For the intermediate composition $0 < x \leqslant 0.1$, strong randomness of the Li doping and the congenital oxygen deficiency cause VRH states even at high temperatures.

1. Introduction

$Li_{1+x}V_3O_8$ is one of several vanadium oxide systems that have received considerable attention as an insertion electrode [1, 2]. This system can accommodate around three or four additional Li ions per formula unit (namely $x = 3$–4) [3].

Using the same atomic labelling scheme as that for $Li_{1.2}V_3O_8$ ($x = 0.2$) [3, 4], the crystal structure of $x = 0.29$ projected on the monoclinic ac-plane, which is refined in this work, is shown in figure 1(a), where the open and shaded circles denote positions at $y = \frac{1}{4}$ and $\frac{3}{4}$, respectively. There exist three crystallographically independent V sites (V1, V2 and V3). The V1 ions apparently have a pyramidal coordination, while the V2 and V3 ions are surrounded octahedrally. The V_3O_8 framework is comprised of the chains of VO_6 octahedra and those of VO_5 pyramids extending along the b-axis. These chains are connected by corner-shared
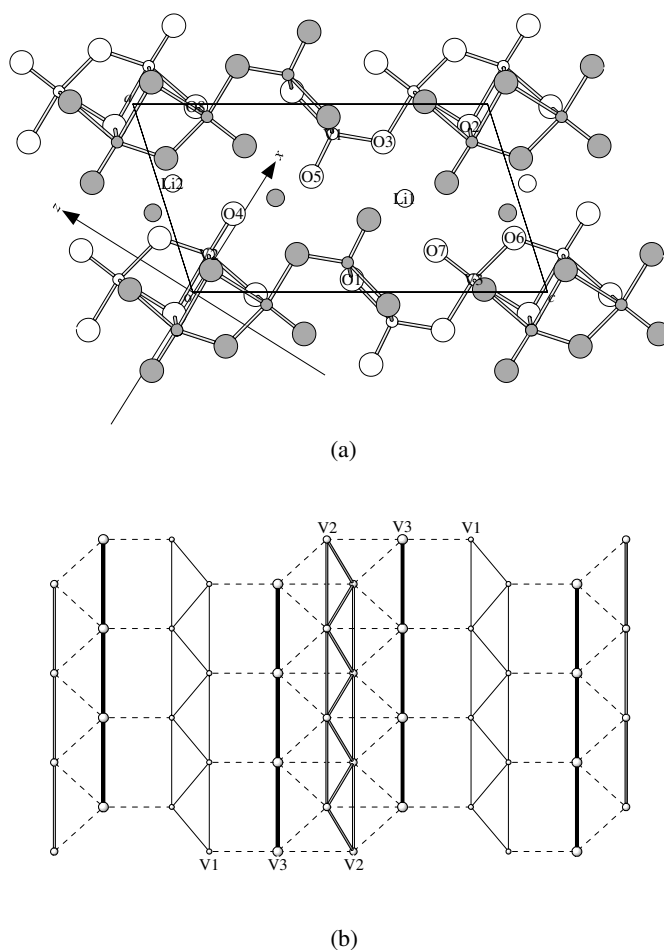
(a)

(b)

Figure 1. The crystal structure of $Li_{1.29}V_3O_8$ at 293 K: (a) the projection on the monoclinic *ac*-plane, where the open and shaded circles denote positions at $y = \frac{1}{4}$ and $\frac{3}{4}$, respectively; $\boldsymbol{x} \parallel 2\boldsymbol{a} + \boldsymbol{c}$, $\boldsymbol{y} \parallel -\boldsymbol{b}$ and $\boldsymbol{z} \parallel \boldsymbol{x} \times \boldsymbol{y}$; and (b) the network of V ions, where the full lines and the dashed ones indicate the paths between the equivalent V sites and those between the inequivalent sites, respectively.

oxygens to lead to continuous sheets of V–O polyhedra. Figure 1(b) indicates the V network, where the full lines and the dashed ones indicate the paths between the equivalent V sites and those between the inequivalent sites, respectively. From this figure, the networks for the equivalent V1 and V2 sites are expressed as zigzag chains and that for the V3 site is a one-dimensional chain. Although the linkage for the inequivalent sites complicates matters, the spin networks responsible for magnetic properties are often simplified due to the symmetry of the ground-state wavefunction for each V site, as recently clarified in δ-phase vanadium bronzes $M_xV_2O_5$ with double-layered structure, where M = Ag or Tl [5, 6]. The Li ions are located predominantly in an octahedral Li1 site (occupancy probability = 1.0). The excess xLi ions reside in a tetrahedral Li2 site as confirmed from the subsequent structural study [3].

In the highly lithiated crystal $Li_4V_3O_8$ ($x = 3.0$), a defect rock-salt structure is formed and all of the Li ions are coordinated octahedrally [3]. The atomic configurations and total energies of $Li_{1+x}V_3O_8$ calculated as a function of x within local-density-functional theory,

using the plane-wave pseudopotential method, are fairly consistent with the results described above [7].

Although the crystal structures and electrochemical properties of the $Li_{1+x}V_3O_8$ system have been investigated in detail, there is little information on the electronic properties as a function of x. In the $M_xV_2O_5$ system, various properties such as polaronic transport, the crossover between the spin-gap state and the linear-chain state or phase transitions are sensitively dependent on the concentration of M [5, 6]. Interesting properties are expected in $Li_{1+x}V_3O_8$ as well, and this work is performed for $0 \leqslant x < 0.4$. Section 2 describes the structural properties characterized by means of single-crystal and powder x-ray diffractions, and in section 3 the electronic properties revealed through measurements of electrical resistivity, thermoelectric power, magnetization and electron paramagnetic resonance (EPR) are discussed. Section 4 is devoted to conclusions.

2. Structural properties

2.1. Sample preparation and lattice constants

Polycrystalline specimens of $Li_{1+x}V_3O_8$ with the nominal range $0 \leqslant x \leqslant 0.50$ were prepared by the solid-state reaction method as follows. First, Li_3VO_4 was obtained by heating a mixture of $3Li_2CO_3$ (99.99%) and V_2O_5 (99.99%) at 823 K for 20 h, and V_2O_3 was made according to the procedure described in [8]. Then, mixtures of $\frac{1+x}{3}Li_3VO_4$, $\frac{16-5x}{12}V_2O_5$ and $\frac{x}{4}V_2O_3$ were ground and pressed into pellets. These were sealed in quartz tubes in Ar atmosphere and then heated at 883 K for 10 h. A preparation of the single crystals with the nominal composition LiV_3O_8 was also done by the Bridgman method from the melt at 883 K with a mixture of Li_2CO_3 and $3V_2O_5$ in air. For the prepared specimens, an x-ray powder diffraction was performed at room temperature using a Rigaku RAD-IIC diffractometer with Cu Kα radiation.

For the specimens with nominal compositions of $0 \leqslant x < 0.4$ the x-ray powder diffraction patterns indicated the single phase, while for those with $0.4 \leqslant x \leqslant 0.5$ impurity phases of LiV_2O_5 and $LiVO_3$ appeared. A preparation of more lithiated specimens needs an electrochemical method. Figures 2(a)–(e) show the composition dependences of the lattice constants at room temperature. The results for crystals from the melt are indicated by crosses, and those in [4] and this work, both determined by the x-ray four-circle diffraction, are plotted by triangles and full circles, respectively. For $x \leqslant 0.3$, as x increases, the a- and b-constants increase significantly and the c-constant does a little, while the β-angle decreases slightly. Therefore, the interlayer distance varies sensitively on Li doping. On the other hand, for the larger x, the lattice constants are nearly x independent. Thus, the volume V increases linearly for $x \leqslant 0.3$, while for the larger x it does not depend on x, indicating that a simple Vegard law appears to be valid in the region of up to about 0.3.

2.2. Effective valences of V ions

For small single crystals with nominal composition $x = 0$ and 0.3 made by the solid-state reaction, the x-ray four-circle diffraction measurements were performed with DI-XRD CAD4 and Rigaku AFC-7R (custom made), respectively. The structural framework refined here[1] essentially corresponds to the previous one for $x = 0.2$ [3]. It should be noted that in this work, the atomic coordinates and isotropic thermal parameter for the Li2 atom in both the crystals are determined precisely *without any constraint*. For both the compositions, Li1 sites are assumed to be occupied fully. The occupancy probabilities of Li2 for $x = 0$ and 0.3 are

---

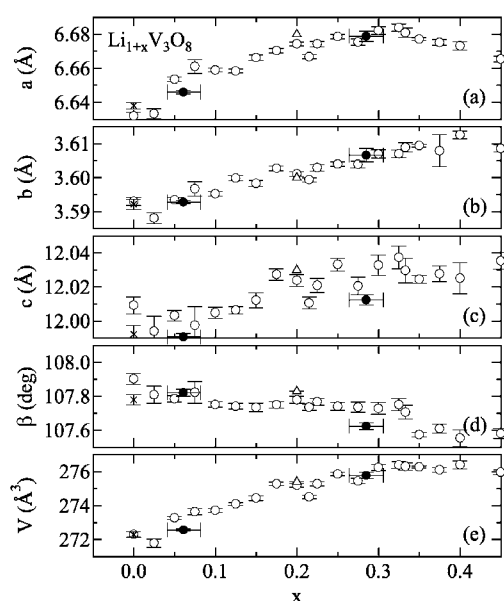[1] Supplementary data files are available from the article's abstract page in the online journal; see http://www.iop.org.

Figure 2. The composition dependences of the lattice constants of $Li_{1+x}V_3O_8$, where open circles indicate the powder diffraction data for specimens prepared by the solid-state reaction; crosses are for those from the melt; and triangles and full circles show the results in [4] and this work on the basis of the x-ray four-circle diffraction, respectively.

$x' = 0.06(2)$ and $0.29(2)$, respectively, which indicates that the composition for the larger x agrees well with the nominal one within a standard deviation. On the other hand, the Li concentration for the lower x seems to be slightly larger than the nominal value. Comparing the equivalent isotropic thermal parameters in $x' = 0.06$ with those in $x' = 0.29$, the value for V3 ion in the former is significantly larger than that for the latter probably due to the slight deficiency of V3 ions. The occupancy probability of V3 ions for $x' = 0.06$ is then estimated to be $0.985(2)$, which leads to the exact chemical formula, $Li_{1.06}V_{2.99}O_3$. As seen in figures 2(a)–(e), the lattice constants plotted against x' estimated from the structure analysis are consistent with the composition dependence based on the powder diffraction data, although possible deficiency of other atoms is not considered. Sizable crystals with $x = 0$ prepared by the solid-state reaction are expected to have the Li concentration slightly larger than x. For single crystals characterized by the structure analysis, the Li concentrations based on the occupancy probabilities are used below. On the other hand, the single crystals with $x = 0$ prepared from the melt seem to have no Li2 atoms, judging from the result in figures 2(a)–(e).

Selected interatomic distances are listed in table 1 with the previous result [3]. On the basis of the bond-length–bond-strength relation [9], the effective valences of V ions are estimated as listed in this table, where the V3 valence for $x = 0.06$ is obtained considering its occupancy probability. The distances and valences for $x = 0.2$ are recalculated with our cell parameters, $a = 6.674(1)$, $b = 3.6010(6)$, $c = 12.023(3)$ Å and $\beta = 107.78(2)°$, since the parameters in [3] are significantly different from our values. The average V valences expected from the chemical formula are 4.99, 4.93 and 4.90 for $x = 0.06$, 0.20 and 0.29, respectively, which agree roughly with the average values for each effective valence. For all of the compositions, the V1 ion is considered to be nearly pentavalent and the V3 is in a mixed valent state of V^{4+} and V^{5+}. In particular, for $x = 0.20$ and 0.29, donated electrons are mainly located at

Table 1. Selected V–O distances (Å) and V valences of $Li_{1+x}V_3O_8$ at room temperature, where the symmetry operators are (i) x, y, z; (ii) $1 - x, -\frac{1}{2} + y, 1 - z$; (iii) $1 - x, \frac{1}{2} + y, 1 - z$; (iv) $1 + x$, y, z; (v) $-1 + x, y, -1 + z$; (vi) $x, y, -1 + z$; (vii) $-1 + x, y, z$.

	$x = 0.06(2)$	$x = 0.20^a$	$x = 0.29(2)$
$V1O_6$ octahedra[b]			
V1(i)–O1(ii, iii)	1.889(1)	1.892	1.896(2)
V1(i)–O1(iv)	1.992(2)	1.993	1.980(2)
V1(i)–O3(i)	1.736(2)	1.730	1.738(2)
V1(i)–O5(i)	1.613(2)	1.603	1.615(3)
V1(i)–O7(iv)	2.798(2)	2.831	2.831(3)
V1 valence	4.97(1)	5.02	4.93(2)
$V2O_6$ octahedra			
V2(i)–O2(v)	2.331(2)	2.332	2.336(2)
V2(i)–O2(ii, iii)	1.884(1)	1.885	1.885(2)
V2(i)–O4(i)	1.614(2)	1.602	1.613(2)
V2(i)–O6(vi)	1.742(2)	1.731	1.742(2)
V2(i)–O8(vii)	2.140(2)	2.127	2.103(2)
V2 valence	4.91(1)	5.02	4.94(1)
$V3O_6$ octahedra			
V3(i)–O2(vii)	2.222(2)	2.231	2.217(2)
V3(i)–O3(vii)	2.014(2)	2.008	1.998(2)
V3(i)–O6(i)	1.917(2)	1.962	1.974(2)
V3(i)–O7(i)	1.608(2)	1.605	1.607(2)
V3(i)–O8(ii, iii)	1.867(1)	1.871	1.874(2)
V3 valence	4.84(1)[c]	4.68	4.66(1)

[a] For $x = 0.2$, the interatomic distances are calculated on the basis of the atomic coordinates listed in [3] and the lattice constants given in the present work (figures 2(a)–(d)).
[b] A long V–O distance is added.
[c] It is estimated with the occupancy probability of V3 atoms.

the V3 site. The V2 ion seems to have a mixed valence just for $x = 0.06$. Using the Hartree–Fock function for V^{4+} [10], the ground-state wavefunctions in the $V1O_6$, $V2O_6$ and $V3O_6$ octahedra for $x = 0.29$ are calculated to be $0.898d_{yz} - 0.439d_{xy}$, $0.999d_{yz} - 0.023d_{xy}$ and $0.999d_{xy} - 0.038d_{yz}$, respectively, where $x \parallel 2a + c$, $y \parallel -b$ and $z \parallel x \times y$ as shown in figure 1(a).

3. Electronic properties

3.1. Electrical resistivity and thermoelectric power

3.1.1. LiV_3O_8 single crystals. The electrical resistivities ρ for the a^*-, b- and c-axis directions of LiV_3O_8 prepared from the melt were measured by a dc four-terminal method in the temperature region between 80 and 500 K. The resistivities as a function of the inverse temperature are shown in figure 3. Here, no thermal hysteresis was observed. All of the directions basically exhibit semiconducting conduction, since the present specimen is nominally a band insulator. There is a large anisotropy of the resistivities: $\rho(a^*){:}\rho(b){:}\rho(c) \simeq 350{:}1{:}90$ at room temperature as expected from the structural characteristics. The mobility for the b-axis at room temperature is 3×10^{-3} cm^2 V^{-1} s^{-1} if the carrier density is about 10^{-1} per formula unit, suggesting a small-polaron conduction. At high temperatures, the thermal variation is nearly expressed by
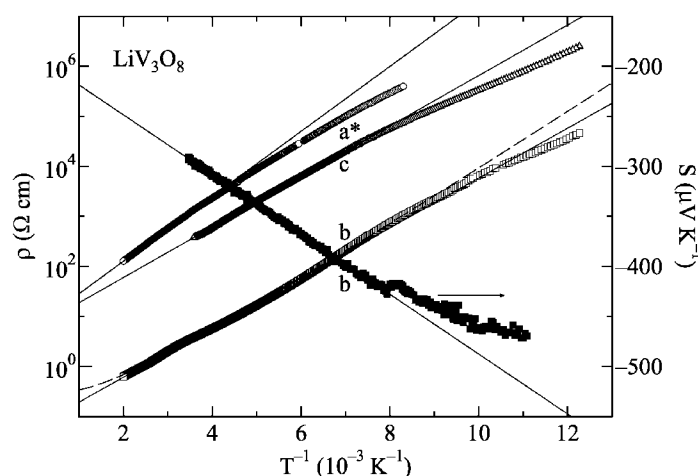
$$\rho = \rho_0 \exp(E_\rho/T) \tag{1}$$

Figure 3. The temperature dependences of the electrical resistivities ρ for the a^*-, b- and c-axis directions, and the thermoelectric power S for the b-axis of LiV_3O_8 prepared from the melt, where the full lines show fits to equations (1) and (2), and the dashed line is that to equation (1) with $\rho_0 \propto T$.

where ρ_0 is assumed to be a constant and E_ρ is a gap. The full lines shown in figure 3 provide $E_\rho = 1495(1), 1146(1)$ and $1162(1)$ K for the resistivities along the a^*-, b- and c-axis, respectively. The anisotropy of the gap is not significant. As found in this figure, the gap at low temperatures appears to decrease, which may be attributed to a variable-range hopping (VRH) mechanism.

The dc measurements of thermoelectric power S for the b-axis of LiV_3O_8 were performed at temperatures between 80 and 300 K. The data against the inverse temperature shown in figure 3 indicate semiconducting behaviours and electron carrier conduction. On the basis of the full line in figure 3, the gap E_S and the temperature-independent value S_0, empirically defined by

$$S = -eE_S/T + S_0 \tag{2}$$

are estimated to be $346.9(8)$ K and $-188.8(3)$ μV K^{-1}, respectively.

The significant difference between E_ρ and E_S may be characteristic of small-polaron motion. It is understood by considering the narrow tails of localized states which extend into the forbidden gap and a band of compensated levels originating from the oxygen deficiency near the middle of the gap. Thus, E_S in equation (2) corresponds to the width between the energies at the Fermi level and at the tail edge, and E_ρ in equation (1) is the sum of the energies for carrier creation and for hopping. Strictly speaking, ρ_0 in equation (1) has weak temperature dependences linear in T and $T^{3/2}$ for the adiabatic and nonadiabatic cases, respectively. The fit for the adiabatic case is shown by the dashed line in figure 3, where E_ρ is $1513(2)$ K for the b-axis.

3.1.2. $Li_{1+x}V_3O_8$ polycrystals. The dc measurements of resistivities with the four-terminal method for the polycrystalline specimens were made at temperatures between 100 and 300 K. Figure 4(a) shows the data against inverse temperature for several compositions. At high temperatures, the temperature dependence follows equation (1) with $E_\rho \approx 2 \times 10^3$ K for $x \leqslant 0.2$ and $E_\rho = 2826(10)$ K for $x = 0.3$ as indicated by the full lines. On the other
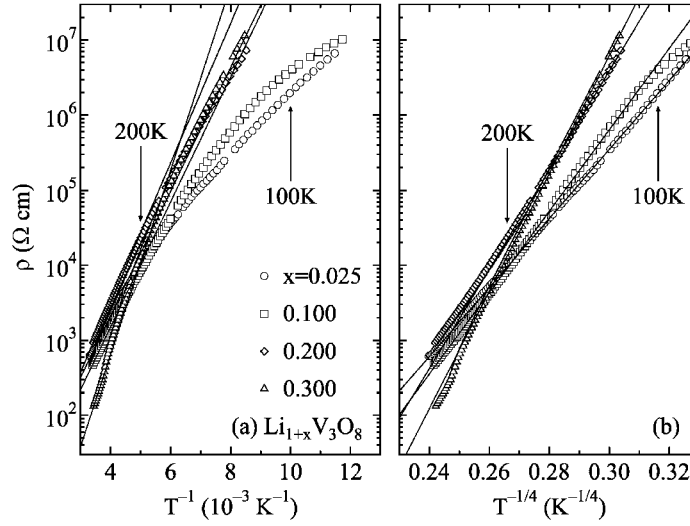
Figure 4. The temperature dependences of the electrical resistivities ρ for several polycrystalline specimens of $Li_{1+x}V_3O_8$, where the full lines in (a) and (b) show plots based on equations (1) and (3), respectively.

hand, at low temperatures, the thermal variations of resistivities with $x \leqslant 0.1$ become weak and deviate from the full lines due to the VRH mechanism. Since the present specimens are polycrystalline, the three-dimensional model is applied (figure 4(b)):

$$\rho = \rho'_0 \exp[(T_0/T)^{1/4}] \tag{3}$$

where ρ'_0 is a constant and T_0 is equal to α^3/n, α and n representing the envelope of the wavefunction as $\exp(-\alpha r)$ and the density of states for the hopping, respectively [11]. From the full lines in figure 4(b), the T_0 values for $x = 0.025$, 0.1 and 0.2 are estimated to be $1.257(3) \times 10^8$, $2.43(1) \times 10^8$ and $5.36(1) \times 10^8$ K, respectively. Thus, T_0 increases with increasing x. When the energy range around the Fermi level for the 3d orbital distribution is smaller than 1 eV, the localization length α^{-1} is estimated to be smaller than 10^{-1} Å, which indicates a strong localization. The resistivity with $x = 0.3$ exhibits a significant increase at around 250 K, below which it follows the 3D VRH model with $T_0 = 1.061(2) \times 10^9$ K.

The thermoelectric powers for the polycrystalline specimens measured with a dc method at temperatures between 100 and 300 K are shown against the inverse temperature in figures 5(a) and (b). They indicate that all of the specimens are nonmetallic as expected from the resistivity result. At high temperatures, the data have a negative sign, which suggests electron carrier conduction. Notwithstanding the polycrystalline specimens, the result for $x = 0$ agrees with that for the single-crystal specimens with finite gap E_S. In contrast, for $0 < x \leqslant 0.2$, the thermoelectric power is nearly temperature independent in the measurement region. For the larger x, it is nearly constant at high temperatures, while at low temperatures it has a tendency to converge to a different value. The composition dependence of the thermoelectric power at room temperature is shown in figure 6.

As described in the previous section, the gap for $x = 0$ may correspond to the carrier-creation energy for the small polaron. The effective valence distributions revealed by the structure analysis indicate that the V sites responsible for the hopping are V2 and V3 for $x = 0.06$, and V3 for $x = 0.29$. For the composition with $x \neq 0$, E_S appears to be about zero.
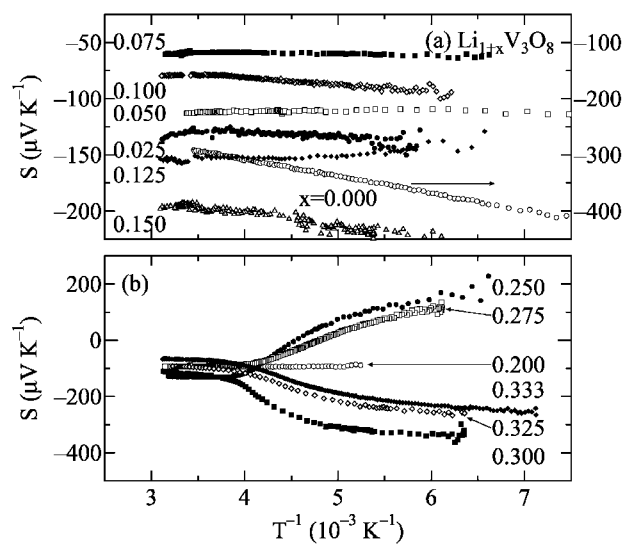
Figure 5. The temperature dependences of the thermoelectric powers S for the polycrystalline specimens of $Li_{1+x}V_3O_8$ with (a) $0 \leqslant x \leqslant 0.15$ and (b) $0.2 \leqslant x \leqslant 0.333$.
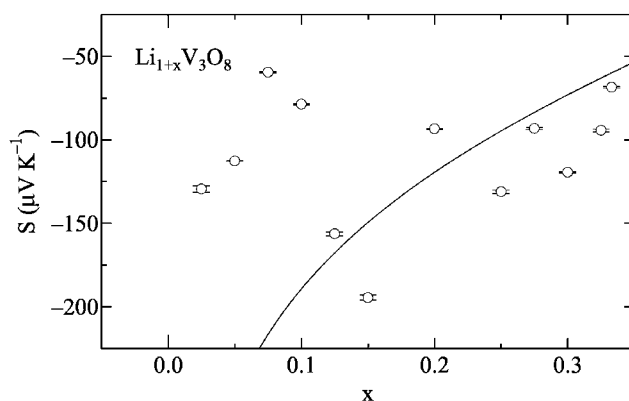

Figure 6. The composition dependence of the thermoelectric power S at room temperature for the polycrystalline specimens of $Li_{1+x}V_3O_8$, where the full curve is drawn on the basis of equation (4).

Then, using the Heikes formula [12],

$$S_p = \frac{k}{e} \ln\left(\frac{x}{N-x}\right) \tag{4}$$

where k is the Boltzmann coefficient and N is the number of V sites for the hopping, the calculated result with $N = 1$ is shown in figure 6 by the full curve. For $x > 0.1$, this model accounts for the experimental results, which justifies our idea that the small polaron for larger x exists mainly in the V3 site. On the other hand, it is difficult to explain the results for $0 < x \leqslant 0.1$ in terms of that model. This discrepancy may be partly attributed to the existence of additional carriers due to the oxygen deficiency, as will be also pointed out from magnetization measurements.
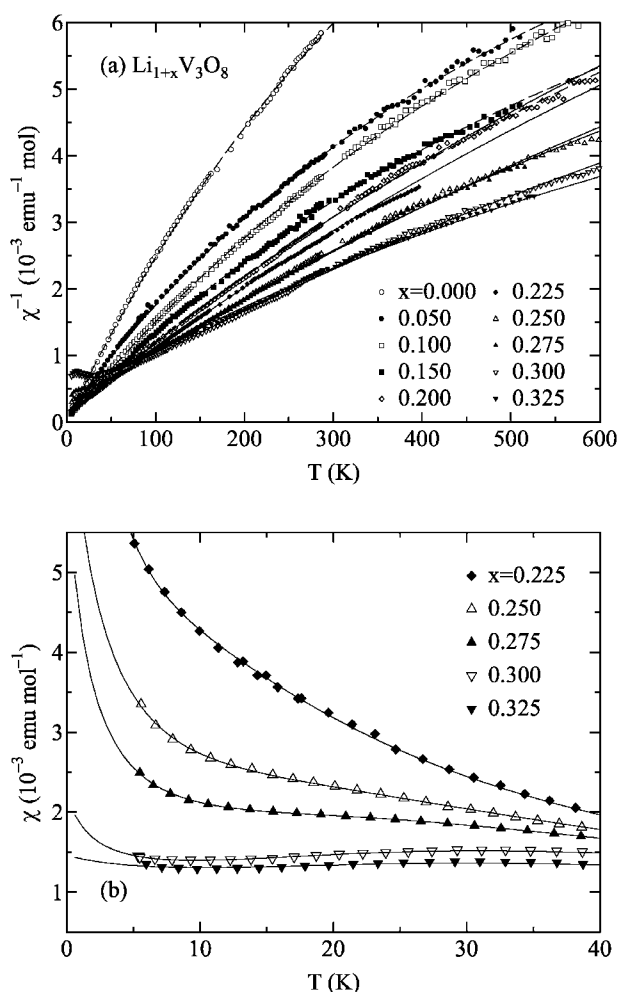
Figure 7. The temperature dependences of (a) the inverse magnetic susceptibility χ^{-1} and (b) χ at low temperatures for $0.225 \leqslant x \leqslant 0.325$, where the dashed curves in (a) are drawn using equation (5) and the full curves in (a) and (b) are done on the basis of equation (6) with the parameters shown in figures 8(a)–(c).

Preliminary nuclear magnetic resonance measurements for $x = 0.25$ indicate that the ionic motion of Li changes at temperatures where the sign of thermoelectric power varies probably due to the large Coulomb repulsion between adjacent Li2 sites. Therefore, the transport anomalies for the large x may be attributed to the order–disorder effect of Li ions.

3.2. Magnetization

The magnetizations of the polycrystalline specimens of $Li_{1+x}V_3O_8$ were measured by the Faraday method with a field of up to 1 T between 4.2 and 600 K. Both cooling and heating processes were examined. The magnetic susceptibility χ was deduced from the linear part of the magnetization-field ($M–H$) curve with a decreasing field.

Figure 7(a) shows the χ^{-1} data as a function of temperature. Here, measurements above 300 K for $x = 0$ gave rise to thermally irreversible results to suffer a loss of oxygen atoms,
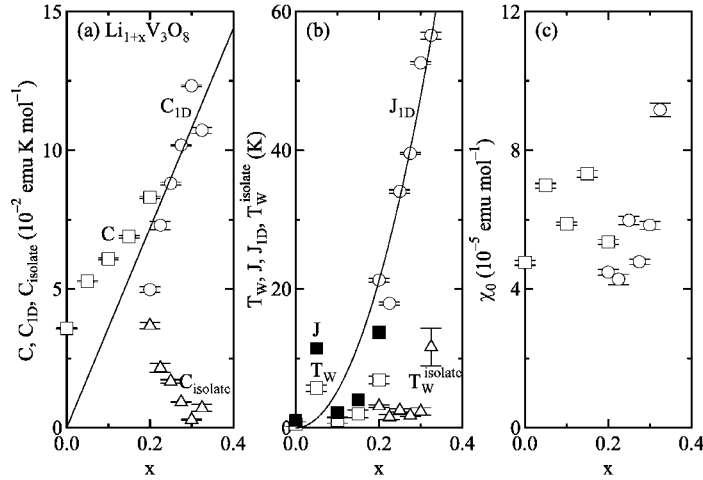
Figure 8. The composition dependences of the parameters in equations (5) and (6): (a) the Curie constants C, C_{1D} and $C_{isolate}$; (b) the Weiss temperatures T_W and $T_W^{isolate}$ and the exchange-coupling constants J_{1D} and J and (c) the constant susceptibilities χ_0. Here, the full line in (a) and the curve in (b) are drawn with $C = 0.36x$ and $J_{1D} \propto x^2$, respectively.

which was directly confirmed by thermogravimetric analysis (not shown). For $0 \leqslant x \leqslant 0.2$, the susceptibility increases monotonically with decreasing temperature and follows a Curie–Weiss law,

$$\chi = \frac{C}{T + T_W} + \chi_0 \tag{5}$$

where C is the Curie constant, T_W is the Weiss temperature and χ_0 corresponds to the temperature-independent susceptibility of the Van Vleck orbital and diamagnetic components. The dashed curves with equation (5) in figure 7(a) are drawn on the basis of the parameters (open squares) plotted in figures 8(a)–(c).

For $x > 0.2$, the temperature dependence of χ does not reflect transport anomalies at around 250 K, and it deviates from the Curie–Weiss law at low temperatures. In particular, for $x \geqslant 0.3$, a round maximum appears at low temperatures as shown in figure 7(b). This indicates that the interaction between 3d spins increases with x and the low-dimensional effects due to the preferential reduction of V ions expected from the crystal structure become significant. A Curie-like tail at the lowest temperatures may come from a phase such as an inevitable lattice imperfection or a magnetic impurity that cannot be detected by standard x-ray powder diffraction. Thus, the susceptibility is described in the form of

$$\chi = \chi_{1D} + \chi_{isolate} + \chi_0 \tag{6}$$

where χ_{1D} is the susceptibility for an $S = \frac{1}{2}$ chain system with the parameters of the Curie constant C_{1D} and the exchange coupling J_{1D}^2 [13], and $\chi_{isolate}$ is the Curie–Weiss-type susceptibility of the isolated V^{4+} ions with $C_{isolate}$ and $T_W^{isolate}$. The full curves with equation (6) in figures 7(a) and (b) are drawn for the parameters (open circles and triangles) plotted in figures 8(a)–(c). This analysis may also be applicable to the data with the lower x, but for the precise estimate of the parameters, measurements at the lower temperatures are needed, since J_{1D} is expected to be rather small. For $x = 0.2$, both analyses with equations (5) and (6) are performed.

---

[2] The Heisenberg Hamiltonian is defined as $H = \sum_{\langle i,j \rangle} J S_i \cdot S_j$, S_i being the spin operator at site i.
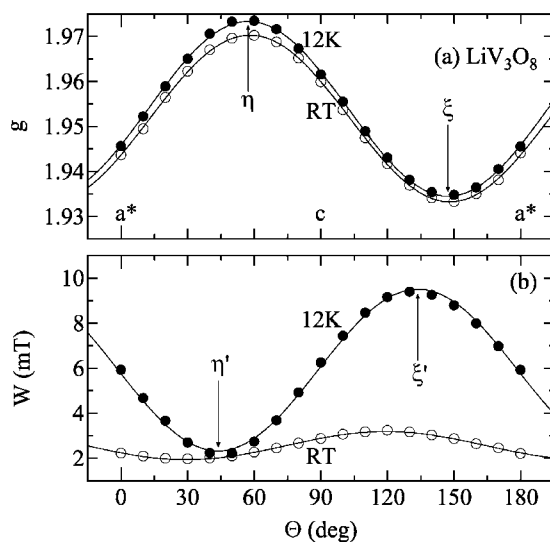
Figure 9. The angular dependences of (a) the g-factors and (b) the EPR linewidths W of LiV_3O_8 single crystals prepared from the melt, at room temperature and 12 K. The full curves in (a) and (b) indicate fits to equations (7) and (8), respectively.

Since the V^{4+} ions have the average g-factor of 1.96 or 1.95 as will be described in section 3.3, the Curie constants for $x > 0.1$ in figure 8(a) agree with the values $C \simeq 0.36x$ (full line) expected from a model where the Li doping with x gives rise to unpaired electrons with x for V ions. Thus, in this x region, the oxygen deficiency is small; especially for $x \geqslant 0.2$, it is negligible. On the other hand, for $0 \leqslant x \leqslant 0.1$, the Curie constants deviate from the full line and the effect of oxygen vacancies is relatively large. Taking the chemical formula as $Li_{1+x}V_3O_{8-\delta}$, δ for $x = 0$ is estimated to be about 0.05.

In the molecular field approximation, the exchange coupling or the Weiss temperature should be proportional to x^2 when the d electrons donated by the Li doping and/or the oxygen deficiency are localized at a specified site. In effect, the composition dependence of J_{1D} for $x > 0.2$, where the oxygen deficiency is nearly absent, is expressed by the formula $J_{1D} \simeq 530x^2$, as shown by the full curve in figure 8(b). Assuming the 1D exchange coupling for $x \leqslant 0.2$, that is, $J = 2T_W$, its composition dependence is obtained as indicated by the full squares in figure 8(b). This behaviour for $x < 0.1$ seems to be explained considering an effective spin-concentration donated by excess Li as well as oxygen deficiency. Alternatively, in this x region, the significant exchange path would be different from the 1D path for $x > 0.2$.

3.3. Electron paramagnetic resonance

3.3.1. LiV_3O_8 single crystals. EPR measurements for the LiV_3O_8 single crystals prepared from the melt were performed in the heating process at temperatures between 12 and 300 K at 9.04 GHz using a JEOL spectrometer. The spectra were symmetric Lorentzian and the spin susceptibility extracted on the basis of the integration of the signal, taking account of the temperature dependence of a Q-factor, agreed well with the magnitude of $\chi - \chi_0$ in equation (5).

The angular dependences of the g-factor and the peak-to-peak linewidth W of the absorption derivative in the a^*b-, ac- and bc-planes were measured at various temperatures. The results of g in the ac-plane at room temperature and 12 K are shown in figure 9(a) and
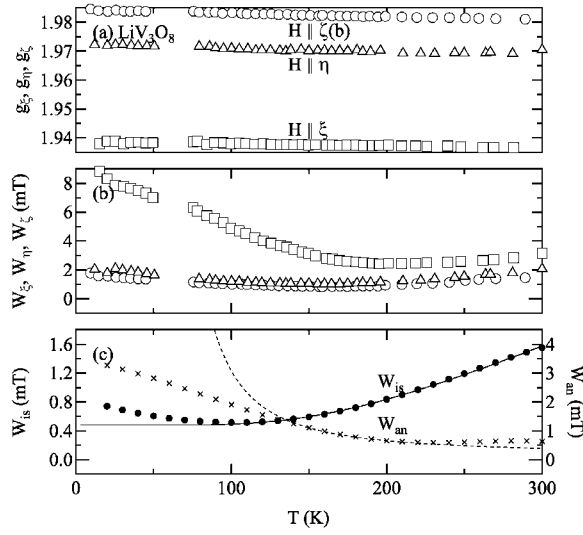
Figure 10. The temperature dependences of (a) the g-factors g_ξ, g_η and g_ζ, (b) the EPR linewidths W_ξ, W_η and W_ζ and (c) their isotropic and anisotropic components W_{is} and W_{an} of LiV$_3$O$_8$ single crystals prepared from the melt. The full and dotted curves in (c) indicate fits with thermally excited frequencies.

those of W are indicated in 9(b). The anisotropy of g is expressed by

$$g^2 = g_\xi^2 \cos^2 \phi \sin^2 \theta + g_\eta^2 \sin^2 \phi \sin^2 \theta + g_\zeta^2 \cos^2 \theta \qquad (7)$$

where θ and ϕ are the polar and azimuthal angles of the direction of the external field, respectively, with respect to the principal axes ξ, η and ζ, ζ corresponding to the b-axis. As shown in figure 9(a), the angle between ξ and a^* is 30(2)°. The temperature dependence of the principal values with $g_\zeta > g_\eta > g_\xi$ is shown in figure 10(a).

The anisotropy of W is given by

$$W = W_{\xi'} \cos^2 \phi \sin^2 \theta + W_{\eta'} \sin^2 \phi \sin^2 \theta + W_{\zeta'} \cos^2 \theta \qquad (8)$$

where the principal axis ζ' is parallel to b, and the angle between ξ' with maximum width and a^* is 45(2)° at 12 K and 60(2)° at room temperature as indicated in figure 9(b). Thus, the directions of the principal tensor for W depend a little on temperature. The linewidths against temperature in the directions of the principal axes for g are shown in figure 10(b).

The energy-level configuration for V^{4+} may be calculated in terms of a simple perturbation theory of the spin–orbit coupling [14]:

$$\Delta g_i = 2\lambda \sum_n \frac{|\langle n|L_i|0\rangle|^2}{E_n - E_0} \qquad (9)$$

where $\Delta g_i = 2 - g_i$; λ is the spin–orbit coupling constant, L_i is the orbital angular momentum operator and E_n is the energy of the orbital state n. Considering the energy levels obtained from the crystal-field analysis[3], the g-tensors described above apparently correspond to those at the V2 site with significant reduction of λ due to covalency effects. With $|0\rangle = d_{yz}$, the energy levels of d$_{zx}$ and d$_{xy}$ orbitals are 67λ and 105λ, respectively. It should be noted that

---

[3] Five orbital states for the V2 site are $0.999d_{yz} - 0.023d_{xy}$, $-0.999d_{xy} - 0.023d_{yz}$, $-0.873d_{zx} - 0.401d_{3z^2-r^2} - 0.276d_{x^2-y^2}$, $0.663d_{3z^2-r^2} + 0.569d_{x^2-y^2} - 0.485d_{zx}$ and $-0.774d_{x^2-y^2} + 0.631d_{3z^2-r^2} - 0.045d_{zx}$ with respective energies -4.2, -2.0, -1.7, 1.7 and 6.1 in a unit of 10^3 K.

the electrons for $x = 0.06$ located at the V2 and V3 sites, and those for $x = 0.29$ are mainly at the V3 site. In contrast, for the nominally Li-undoped specimens, the magnetic site is mainly V2.

The EPR relaxation is basically due to the random frequency modulation of the hyperfine interaction A_{hf} with two characteristic frequencies [15], as performed for the slightly oxygen deficient Ag$_2$V$_4$O$_{11}$ insertion electrode [16]. The hopping frequency ν_1 is expected to be larger than A_{hf} at the lowest temperature, since hyperfine spectra are not resolved. Another frequency ν_2 is responsible for a transition of electrons into a certain excited state. In the measurement region, the difference between $W_{\xi'}$ ($W_{\zeta'}$) and the linewidth along ξ (ζ) is small, so the results shown in figure 10(b) are roughly regarded as those of the principal values of linewidth. In addition, for simplicity, the directions of ξ' and η' for the linewidths that depend on temperature are assumed to coincide with those of ξ and η for the g-factors. Thus, the temperature dependence of ν_1 may be qualitatively estimated from that of the anisotropic component of the linewidth defined as $W_{an} = (2W_{\xi'} - W_{\eta'} - W_{\zeta'})/4$. Then, using the hyperfine interaction parameters for dilute V^{4+} ions in V$_2$O$_5$ [17], the isotropic component (W_{is}) of the linewidth due to just ν_2 can be evaluated from the relation $W_i = W_{is} + \gamma A_{hf}^{i}{}^2/\nu_1$ with constant γ for $i = \xi, \eta$ and ζ. Assuming that ν_2 has the temperature dependence

$$\nu_2 \propto \exp(-\Delta_2/T) \tag{10}$$

the energy Δ_2 is estimated to be 700 K as shown by the full curve in figure 10(c). Above 140 K, ν_1 also has a similar temperature dependence with $\Delta_1 \simeq 300$ K as indicated by the dotted curve. The values of Δ_1 and Δ_2 obtained above roughly agree with those of E_S and $E_\rho - E_S$ in section 3.1. At low temperatures, on the other hand, ν_1 is not of thermally excited type due to the finite local electron hopping between localized states. In effect, in this temperature region, the electrical conduction is of VRH type as suggested in section 3.1.

3.3.2. Li$_{1+x}$V$_3$O$_8$ polycrystals.

The EPR spectra for the Li$_{1+x}$V$_3$O$_8$ polycrystalline specimens were measured by the same method as described before. The spectra were asymmetric and the spin susceptibilities extracted from the signal corresponded to the magnitude of $\chi - \chi_0$ in equations (5) and (6). The spectra are approximately explained on the assumption that g and W with a Lorentzian shape have the uniaxial angular dependences with respective principal values $g_{Z(XY)}$ and $W_{Z(XY)}$ parallel (perpendicular) to the principal axis Z. The composition dependences of g_{XY} and g_Z at room temperature (the open symbols) and about 40 K (the full ones) are shown in figure 11(a), and those of W_{XY} and the anisotropy W_Z/W_{XY} are in 11(b) and (c), respectively. Here, for comparison, the results for LiV$_3$O$_8$ polycrystals are indicated, which are compatible with those for the single crystals prepared from the melt. For polycrystalline specimens with $x = 0.07$, the following results were reported without considering the anisotropy of linewidth: $g_{XY} = 1.96$ and $g_Z = 1.94$ at 77 K [18], which are a little different from the present results[4].

For $0 < x \leqslant 0.275$ and $x \geqslant 0.3$, the space-averaged g-factors $\langle g \rangle$ are nearly 1.96 and 1.95, respectively, as described in section 3.2. A slight deviation from the spin-only value is attributed to the second-order perturbation in equation (9) for V^{4+} with singlet ground-state orbital. The energy-level configurations for small and large x should be estimated considering

---

[4] On the basis of figure 3 in [18], the analyses of EPR spectra assuming a frequency of 9 GHz provide the following results: for Li$_{1.07}$V$_3$O$_{7.94}$ prepared at 953 K, $g_{XY(Z)} = 1.980\,(1.933)$ and $W_{XY(Z)} = 6.62\,(9.03)$ mT at 293 K, and $g_{XY(Z)} = 1.980\,(1.931)$ and $W_{XY(Z)} = 3.55\,(8.69)$ mT at 77 K; for Li$_{1.07}$V$_3$O$_{7.92}$ prepared finally at 623 K, $g_{XY(Z)} = 1.976\,(1.930)$ and $W_{XY(Z)} = 2.79\,(2.91)$ mT at 293 K, and $g_{XY(Z)} = 1.977\,(1.932)$ and $W_{XY(Z)} = 1.62\,(2.65)$ mT at 77 K. The values for the specimens prepared at 623 K are consistent with the present result in figure 11, while those prepared at 953 K seem to correspond to the result with larger x.
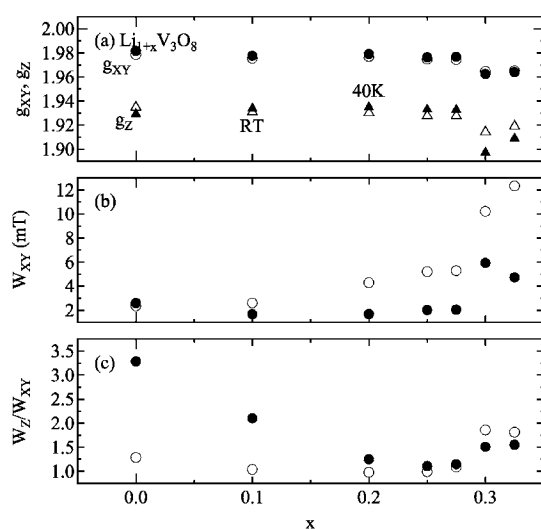
Figure 11. The composition dependences of (a) the g-factors g_{XY} and g_Z; (b) the EPR linewidths W_{XY} and (c) their anisotropy W_Z/W_{XY} of $Li_{1+x}V_3O_8$ polycrystals at room temperature (the open symbols) and 40 K (the full ones).

the susceptibility-weighted means of g-factors at the V2 and V3 site, and those at the V3 site and the isolated site, respectively.

For all of the compositions, the linewidths indicate temperature-dependent behaviours. In addition, for $x > 0.2$ with sizable exchange coupling, the linewidth at room temperature increases significantly with x or J_{1D}. The EPR relaxation for $x = 0$ with just oxygen deficiency is basically understood as described in a previous subsection, while for the Li-doped specimen different contributions of dipole–dipole (dd), anisotropic exchange (ae) and Dzyaloshinsky–Moriya (DM) interactions should be considered. Here, the DM term has been sometimes considered to be responsible for the large linewidth observed in transition-metal oxides with significant J. However, recent theoretical works claim that the DM contribution is only of the same level as the ae one [19, 20], although a quantitative estimate is not obtained. When the method in section 3.3.1 is applied to the data for $x = 0.1$ and 0.2 (not shown) by way of trial, $\Delta_2 \approx 6 \times 10^2$ and 5×10^2 K are obtained, respectively, which are rather small as compared with results based on the transport properties. For $x > 0.2$, on the assumption that the relaxation via the lattice does not depend on the composition, the rapid increase of linewidth with x suggests that the ae and/or DM contributions are relevant to the relaxation mechanism, since $J_{1D} \propto x^2$. In order to clarify these respects, further theoretical works are necessary.

4. Conclusions

The structural and electronic properties of the $Li_{1+x}V_3O_8$ system with the single-phase region $0 \leqslant x < 0.4$ have been investigated from multiple viewpoints.

Detailed refinements of the crystal structures of $Li_{1.06}V_3O_8$ and $Li_{1.29}V_3O_8$ indicate that the doped electrons for $x = 0.06$ are located at the V2 and V3 sites, and those for $x = 0.29$ are at the V3 site. Since no electron resides at the V1 site, the block comprised of V2 and V3, their ground-state orbitals being d_{yz} and d_{xy}, respectively, leads to one-dimensional electronic properties notwithstanding rather complicated structure. For example, the composition with $x = 0.33$ may lead to a $\frac{1}{6}$-filled band in the V3 site.

All of the compositions basically exhibit semiconducting conduction. For $x = 0$, the transport mechanism of 3d electrons at the V2 site donated by the slight deficiency of oxygen atoms is understood as a small-polaron conduction in the localized states of band tails with the hopping energy 700 K and the negative carrier-creation energy 300 K, which is consistent with the result obtained from EPR relaxation. For $x > 0.1$ with nearly full occupancy of oxygen atoms, small polarons exist without carrier-creation energy at high temperatures, while at low temperatures the conduction may be of VRH type due to the atomic randomness. For $x > 0.2$, one-dimensional magnetic properties appear due to sizable exchange couplings between V3 sites, where $J_{1D} \propto x^2$, and order–disorder effects of additional Li ions due to the Coulomb repulsion between adjacent Li2 sites may induce a change of transport properties. For the intermediate composition $0 < x \leqslant 0.1$, strong randomness of the Li doping and the congenital oxygen deficiency causes VRH states even at high temperatures.

This work clearly indicates that the structural as well as electronic properties are very sensitive to the partially reduced state of the insertion electrode. It has been found preliminarily that the initial voltage of second ion batteries with positive electrodes prepared here decreases smoothly with excess Li concentration x. Therefore, it is possible to examine from various viewpoints that the electrodes prepared are put to practical use.

References

[1] Pistoia G, Pasquali M, Tocci M, Moshtev R V and Maner V 1985 *J. Electrochem. Soc.* **132** 281
[2] Kishi T, Kawakita J and Miura T 2000 *Electrochemistry* **68** 2
[3] de Picciotto L A, Andendorff K T, Liles D C and Thackeray M M 1993 *Solid State Ion.* **62** 297
[4] Wadsley A D 1957 *Acta Crystallogr.* **10** 261
[5] Onoda M and Arai R 2001 *J. Phys.: Condens. Matter* **13** 10399
[6] Onoda M and Hasegawa J 2002 *J. Phys.: Condens. Matter* **14** 5045
[7] Benedek R and Thackeray M M 1999 *Phys. Rev.* B **60** 6335
[8] Onoda M, Ohta H and Nagasawa H 1991 *Solid State Commun.* **79** 281
[9] Zachariasen W H 1978 *J. Less-Common Met.* **62** 1
[10] Freeman A J and Watson R E 1965 *Magnetism* part A vol 2, ed G T Rado and H Suhl (New York: Academic)
[11] Brenig W, Döhler G H and Wölfle P 1973 *Z. Phys.* **258** 381
[12] Heikes R R 1961 *Thermoelectricity* ed R R Heikes and R W Ure (New York: Interscience)
[13] Bonner J C and Fisher M E 1964 *Phys. Rev.* **135** A640
[14] Abragam A and Bleaney B 1970 *Electron Paramagnetic Resonance of Transition Ions* (Oxford: Clarendon)
[15] Zimmermann P H 1973 *Phys. Rev.* B **8** 3917
[16] Onoda M and Kanbe K 2001 *J. Phys.: Condens. Matter* **13** 6675
[17] Kahn A, Livage J and Collongues R 1974 *Phys. Status Solidi* a **26** 175
[18] Kosova N V, Anufrienko V F, Vasenin N T, Vosel S V and Devyatkina E T 2002 *J. Solid State Chem.* **163** 421
[19] Choukroun J, Richard J-L and Stepanov A 2001 *Phys. Rev. Lett.* **87** 127207
[20] Oshikawa M and Affleck I 2002 *Phys. Rev.* B **65** 134410
[21] Burla M C, Camalli M, Cascarano G, Giacovazzo C, Polidori G, Spagna R and Viterbo D 1989 *J. Appl. Crystallogr.* **22** 389
[22] teXsan 1992 *Crystal Structure Analysis Package* (The Woodlands, TX: Molecular Structure Corporation)